MULTI-MODEL VARIATION OF THE ENHANCED ASIAN RAINFALL AND CONTINENT-OCEAN THERMAL GRADIENT FROM PRE-INDUSTRIAL TO MID-HOLOCENE

VARIASI MULTI-MODEL PADA PENINGKATAN HUJAN ASIA DAN GRADIEN SUHU BENUA-LAUT DARI PRA-INDUSTRI SAMPAI HOLOSEN TENGAH

Adinda Maharani[1*], Yudha Setiawan Djamil[2], Rima Rachmayani[3]

[1] Program Studi Sains Kebumian, Fakultas Ilmu dan Teknologi Kebumian Institut Teknologi Bandung (ITB), Jl.Ganesha No.10, Bandung, Jawa Barat, Indonesia

[2] Pusat Riset Iklim dan Atmosfer (PRIMA), Badan Riset dan Inovasi Nasional (BRIN), Jl. Dr. Djunjunan No. 133, Bandung, 40173, Indonesia

[3] Kelompok Keahlian Oseanografi, Fakultas Ilmu dan Teknologi Kebumian, Institut Teknologi Bandung (ITB),Jl.Ganesha No.10, Bandung, Jawa Barat, Indonesia

*Corresponding author: adndamahrani@gmail.com

(Received 30 May 2022; in revised from 30 May 2022; accepted 25 August 2022)

DOI : 10.32693/bomg.37.1.2022.762

ABSTRACT : Rainfall over the Asian continent during the mid-Holocene was higher than today as shown by the rainfall proxy records. During the mid-Holocene, increased rainfall over the Asian Continent has been suggested to be associated with the strengthening of the Asian Summer Monsoon (ASM) following a sharper continent-ocean thermal gradient. This study examined multi-model variation between changes of the continent-ocean thermal gradient and the increased rainfall over Asia during the mid-Holocene as compared to the pre-Industrial. We analyzed surface temperature, precipitation, and wind at 850mb from nine Global Climate Models (GCMs) which are all obtained from the database of the Paleoclimate Modeling Intercomparison Project Phase-3 (PMIP3). Multi-model analysis shows that changes in a continent-ocean thermal gradient has a positive correlation with ASM wind. However, a negative correlation occurs between changes in the continent-ocean thermal gradient with Asian rainfall. Models that simulate large changes in the continent-ocean thermal gradient produced the smallest increase in the Asian rainfall and vice versa. Such inverse relation is likely due to the cooling of Indian Ocean SST since its correlation scores with Asian rainfall is much higher than the one with the warming of the Asian continent. Thus, multi-model variation of the increased rainfall over the Asian continent between mid-Holocene and today is mainly related to the multi-model variation of the cooling in the Indian Ocean SST.

Keywords: Asian Summer Monsoon, Indian Ocean, Multi-model, Sea Surface Temperature, PMIP3

ABSTRAK*: Curah hujan di benua Asia selama Holosen Tengah mengalami peningkatan dibandingkan masa sekarang berdasarkan catatan proksi curah hujan. Selama Holosen Tengah, peningkatan curah hujan di Benua Asia diduga berhubungan dengan penguatan fenomena Muson Asia (ASM) di musim panas yang diakibatkan oleh gradien suhu benua-laut yang meningkat. Studi ini mengkaji variasi multi-model antara perubahan gradien suhu benua-laut dan peningkatan curah hujan di Asia saat Holosen Tengah dibandingkan dengan era Pra-Industri. Parameter yang dianalisis adalah suhu permukaan, curah hujan, dan angin 850mb dari sembilan Global Climate Models (GCMs) yang diperoleh dari database Paleoclimate Modeling Intercomparison Project Phase-3 (PMIP3). Analisis multi-model menunjukkan bahwa perubahan gradien suhu benua-samudera memiliki korelasi positif dengan angin ASM. Namun, korelasi negatif terjadi antara perubahan gradien suhu benua-laut dengan curah hujan Asia. Model yang mensimulasikan perubahan terbesar dalam gradien suhu benua-laut menghasilkan peningkatan terkecil dalam curah hujan Asia dan sebaliknya. Hubungan terbalik tersebut kemungkinan disebabkan oleh pendinginan SPL di Samudera Hindia karena skor korelasinya dengan curah hujan Asia jauh lebih tinggi dibandingkan dengan korelasi antara peningkatan hujan dengan pemanasan benua Asia. Dengan demikian, variasi multi-model dari peningkatan curah hujan di benua Asia antara pertengahan Holosen dan masa kini utamanya terkait dengan variasi multi-model dari pendinginan SPL di Samudra Hindia.*

Kata Kunci: *Asian Summer Monsoon, Indian Ocean, Multi-model, Suhu Permukaan Laut, PMIP3*

INTRODUCTION

Mid-Holocene, a period around six thousand (~6,000) years ago (ka), is known as a period with a maximum warm climate phase (Yafeng et al., 1993). During mid-Holocene, increased insolation occurred in the northern hemisphere during boreal summer as compared to the Holocene period (Berger, 1978). The increased insolation strengthened the Asian Summer Monsoon (ASM), which is one of the most fundamental phenomena in the global circulation of the atmosphere (Braconnot et al. 2000; Cheng et al. 2021; Joussaume et al. 1999; Wang and Fan 1999; Zhao et al. 2005). ASM affects the climate in the Asian continent due to the heat and moisture transfer from the ocean to the continent at high latitudes (Chen et al., 2008). ASM is associated with rainfall in the Asian continent, due to the large-scale transport of water vapor from Indian Ocean to Asian Continent (Ding & Chan, 2005; Ohgaito & Abe-ouchi, 2007).

ASM has been suggested to be stronger in the mid-Holocene than today (Rawat et al., 2021). Previous studies on rainfall proxy during the Holocene have suggested that the increased rainfall in Asia during mid-Holocene was due to changes in the interhemispheric thermal gradient during the boreal summer (Cheng et al. 2016a). Moreover, the paleo isotope records of oxygen and deuterium showed increased rainfall in southern and northern China (Rao et al., 2016). Additionally, some pollen and microfossil data revealed an intensified rainfall in most of China (Bartlein et al., 2011). During the mid-Holocene, in northern China, the peak rainfall occurred during boreal summer as indicated by sediment core record of Hulun Lake and Daihai Lake (Wen et al., 2010; Xiao et al., 2009).

In addition to proxy records, numerical simulations were carried out to describe ASM and rainfall conditions in Asia during the mid-Holocene. Wetter-than-today ASM is well-simulated by the Paleoclimate Model Intercomparison Project Phase-2 (PMIP2), which exhibited an enhanced rainfall of East Asia during boreal summer in the mid-Holocene, compared to that of the pre-Industrial (Dallmeyer, 2011; Tao et al., 2010). This is in line with the other simulations of PMIP2, which show rainfall intensification of China during boreal summer in the mid-Holocene by 10.5% than today (Jiang et al., 2013). Thus, model study under PMIP has revealed that the ASM during the mid-Holocene was stronger and wetter than today.

During the mid-Holocene, proxy records and model simulations indicate intensification of ASM and rainfall in Asia as a respond to the enhanced insolation in the northern hemisphere. The increase insolation raises the Asian surface temperature (Polanski et al., 2012). Rising Asian surface temperature changes the thermal gradient between Asian continent and Indian Ocean (Cheng et al. 2016a; Wohlfahrt et al, 2004). Previous studies verified that changes in the inter-hemispheric thermal gradient, lead to a higher rainfall in the northern hemisphere (Schneider et al., 2014). Thus, the difference in the surface temperature gradient in Asian continent and Indian Ocean between during mid-Holocene and today is expected to change the magnitude of ASM.

Many numerical studies were done to understand the mechanisms of the increased Asian rainfall between mid-Holocene and today (Dallmeyer et al., 2011; Hewitt & Mitchell, 1996; Ren et al., 2021; Tao et al., 2010). However, study on multi-model variation (multi-model analyses), in terms of physical quantities associated with stronger-than-today ASM during the mid-Holocene, has not been conducted. Multi-model analysis has been previously used to analyze the general relationship between climate seasonality and ENSO on several paleoclimate scenarios (Emile-Geay et al., 2015). Therefore, the aim of our research is to analyze the multi-model variation from the output of GCMs involved in PMIP3, regarding the shifting impacts in the continent-ocean thermal gradient to the Asian rainfall enhancement between mid-Holocene and pre-Industrial scenarios. This study consists of several sections. Detail specifications of GCM and the methods are described under the section 2. Moreover, Section 3 displays the result from the changes among the physical parameters and their correlations during the mid-Holocene. Section 4 discusses relationship between all physical parameters with suggested mechanisms. Additionally, Summary and conclusions are defined in Section 5. Every section is explained below.

METHODS AND MATERIAL

Data

This study compared simulation output from 9 GCMs based on the mid-Holocene and pre-Industrial climate scenarios. Mid-Holocene scenario is mainly defined by a stronger-than-today insolation in the northern hemisphere during boreal summer (Berger, 1978). Pre-Industrial scenario is a period before industrial revolution (~1850) when the climate was not yet influenced by the rising concentration of greenhouse gases from fossil fuels or known as the anthropogenic forcing (Mahowald et al., 2006). These simulations are part of the Paleoclimate Model Intercomparison Project - Phase 3 (PMIP3), which their output is openly accessible in a website administered by the German Climate Computing Center (cera-www.dkrz.de). The 9 GCMs are BCC-CSM1, CCSM4, CESS FGOAL-S2, CSIRO MK-3-6-0, IPSL-CM5A-LR, MPI ESM-P, MIROC ESM, MRI-CGCM3, and NASA GISS-E2. Physical quantities used in this study are monthly rainfall, surface temperature, and horizontal (zonal and meridional) wind at 850mb. General specification of each GCM is described in Table 1.

Methodology

Stronger-than-today insolation on the northern hemisphere during the mid-Holocene is known to strengthened continent-ocean thermal gradient, ASM wind, and Asian rainfall following the northward

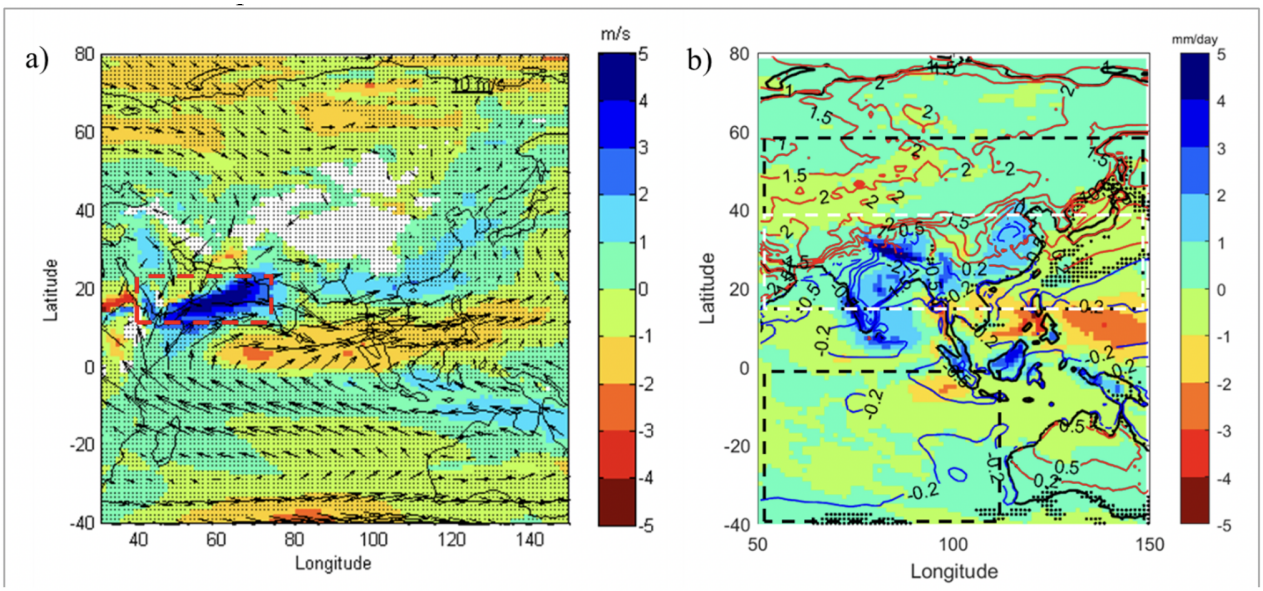

Figure 1. Seasonal mean of (a) the wind magnitude (shaded colour, in m/s) and direction (arrow), (b) the rainfall (shaded color, in mm/day) and surface temperature (contour, in K) during boreal summer for the mid-Holocene minus pre-Industrial simulations by the MRI-CGCM3. Contours in red and blue represent positive and negative changes in temperature respectively. Dotted areas are not significant at 95% confidence level for the rainfall change. Red dashed rectangles are areas to calculate area-averaged of ASM wind, black dashed rectangles are areas to calculate area-averaged of surface

Table 1. General description of the nine GCMs involved in this study. All models are part of the PMIP3 which their simulation output are freely accessible in cera-www.dkrz.de. (https://wiki.lsce.ipsl.fr/pmip3/doku.php/pmip3:database:status).

Model name	**Country**	**Number of horizontal grid and vertical layers**	**Length of simulation per-scenario (Year)**		**Cite**
			pre-Industrial	**mid-Holocene**	
BCC-CSM1	China	128 x 64 x L21	1500	100	(Wu & Xin, 2015)
CCSM4	USA	288 x 192 x L26	1503	903	(Otto-Bliesner, 2014)
CESS FGOALS-S2	UK	192 x 145 x L38	30	30	(LASG 2015)
CSIRO MK-3-6-0	Australia	64 x 56 x L1	1353	153	(Jeffrey et al., 2016)
IPSL-CM5A-LR	Prancis	96 x 95 x L39	2703	1203	(Braconnot et al., 2016)
MIROC ESM	Japan	36 x 43 x L40	277	243	(JAMSTEC et al., 2015)
MPI ESM-P	Japan	196 x 98 x L47	603	273	(Jungclaus et al., 2012)
MRI-CGCM3	Japan	364 x 160 x L48	1203	273	(Yukimoto et al., 2015)
NASA GISS-E2-R	USA	40 x 60 x L40	63	63	(NASA 2014)

migration of Inter-tropical Convergence Zone (ITCZ) in orbital time-scale (Schneider et al., 2014; (Tapio Schneider et al., 2014)Rawat et al., 2021). Changes of all three parameters during boreal summer are defined as the differences in their mean between the two climate scenarios (mid-Holocene minus pre-Industrial) during June, July and August (JJA). The seasonal mean during boreal summer is calculated based on the area averaged within 50E – 150E, 20N-60N for Asian surface temperature, 40E – 70E, 10N-20N for ASM wind, 50E – 150E, 20N-40N for rainfall, and 50E - 150E, 0 – 40S for Indian Ocean SST (Figure 1a & 1b). All these areas are chosen since significant changes relative to its surroundings have been identified. The ASM wind intensity for our study is based on the low-level wind at 850mb since it is also used by the Indian Monsoon index (Wang and Fan, 1999; Wang et al., 2001).

The differences (Δ) between the mid-Holocene (*mH*) and pre-Industrial (*piC*) simulations for the seasonal mean of the surface temperature between Asian Continent and Indian Ocean ($\partial\Delta T$), the ASM wind (ΔAm_{as}) and rainfall over the Asian Continent (ΔP_{as}) are define as follow:

$$\Delta T_{oc} = T_{oc\_mH} - T_{oc\_piC} \quad (1)$$

$$\Delta T_{as} = T_{as\_mH} - T_{as\_piC} \quad (2)$$

$$\partial\Delta T = \Delta T_{as} - \Delta T_{oc} \quad (3)$$

$$\Delta AM_{as} = AM\_mH - AM\_piC \quad (4)$$

$$\Delta P_{a\,s} = P_{as}\_mH - P_{as}\_piC \quad (5)$$

Where T_{oc} and T_{as} are the seasonal mean of the Indian Ocean SST and Asian continent surface temperature, respectively.

Seasonal mean changes of all the above parameters are compared to each other in order to check the consistency of the multi-model variation to the coherency of these parameters as previously suggested (Schneider et al., 2014; Rawat et al., 2021). For example, models with much (less) sharper continent-ocean thermal gradients are hypothesized to produce stronger (weaker) ASM wind and higher (lower) Asian rainfall. Thus, multi-model variations of these comparisons are quantified by calculating linear regressions and Pearson's correlation scores.

RESULTS

Multi-model variation in terms of relationship between continent-ocean thermal gradient (∂ΔT) with Asian monsoon wind (ΔAMas), as well as with continent-ocean thermal gradient is displayed in Figure 2(a). On the other hand, the relationship between continent-ocean thermal gradient and Asian monsoon wind with Asian rainfall presented in Figure 2(b) and 2(c). Continent-ocean thermal gradient consists of Asian surface temperature and Indian Ocean SST. Hence, the relationships of the surface temperature on each location (Asian continent and Indian Ocean) are also presented in Figure 2(c) and 2(d). Temperature changes in each location (Asia and Indian Ocean), continent-ocean thermal gradient, Asian monsoon wind, and Asian rainfall between the mid-Holocene and pre-Industrial simulations are described in Table 2.

Among models, continent-ocean thermal gradient rises with range of 0.83K to 1.45K, similar to the variability of Asian average rainfall which also increases between 0.23 to 0.68 mm/day, and Asian monsoon wind that enhances between 0.35 and 2.45 m/s (Table 2). The seasonal mean change of Asian surface temperature among models also increased by 0.57K to 1.09K, while the Indian Ocean SST relatively drop between (-0.22K) to (-0.63K). All changes are statistically significant at 95% confidence level.

Figure 2 (a) represent the relationship of multi-model variation between the continent-ocean thermal gradient and Asian monsoon wind, which indicate a positive high correlation (R score ~0.78). The range of the changes in the continent-ocean thermal gradient and Asian monsoon wind are between 0.57 to 1.09 K and 0.35 to 2.45 m/s respectively. The smallest change was simulated by GISS E2-R while the largest one was done by MRI CGCM3. GISS E2-R produces the tiniest change of the ocean-continent thermal gradient and monsoon wind at 0.83 K and 0.35 m/s respectively. While MPI-ESM-P shows the largest change of Asian monsoon wind at 2.45 m/s, instead of the ocean-continent thermal gradient.

Figure 2(b) shows multi-model variation between Asian monsoon wind and rainfall. GISS E2-R and CCSM4 indicate discernible distances from the rest on the model. Thus, two regressions were conducted. Solid line is the regression of all models, and dashed line is the regression without GISS E2-R and CCSM4. Both regression lines and correlation scores of the multi-model variation denote negative correlation (correlation score of ~(-0.43) and ~(-0.78) for the solid and dashed line). These suggest that models with much stronger ASM wind is associated with weaken Asian rainfall. The shifting range of Asian rainfall is between 0.19 to 0.68 mm/day. The correlation score without GISS E2-R and CCSM4 is higher compared to that of involving all models.

Figure 2(c) displays multi-model variation between thermal gradient and Asian rainfall. Similar to Figure 2(b), a group of models indicate anti-correlation between the two parameters. The models are: BCC-CSM1, FGOALS-G2, CSIRO MK-3-6-0, IPSL-CM5A-LR, MPI ESM-P, and MRI-CGCM3. The other two models, CSSM4 and

Table 2 Mean of the investigated physical quantities during boreal summer for the mid-Holocene minus pre-Industrial of the nine GCMs. See equations 1 to 5 for the detail calculations. All means are significant at 95% confidence level.

No	Global Model Data	ΔT_{as} (K)	ΔT_{oc} (K)	$\partial\Delta T$ (K)	ΔP_{as} (mm/day)	ΔAM_{as} (m/s)
1	BCC-CSM1	1.03	-0.42	1.45	0.27	2.16
2	CCSM4	0.70	-0.32	1.02	0.25	0.74
3	FGOALS G2	0.84	-0.63	1.47	0.19	2.14
4	CSIRO MK3-6-0	1.09	-0.22	1.32	0.68	0.91
5	IPSL CM5A	0.99	-0.34	1.33	0.43	1.62
6	MIROC ESM	0.72	-0.60	1.32	0.47	0.69
7	MPI ESM P	0.77	-0.37	1.14	0.56	1.22
8	MRI CGCM3	1.08	-0.32	1.40	0.37	2.45
9	NASA GISS E2 R	0.57	-0.26	0.83	0.41	0.35

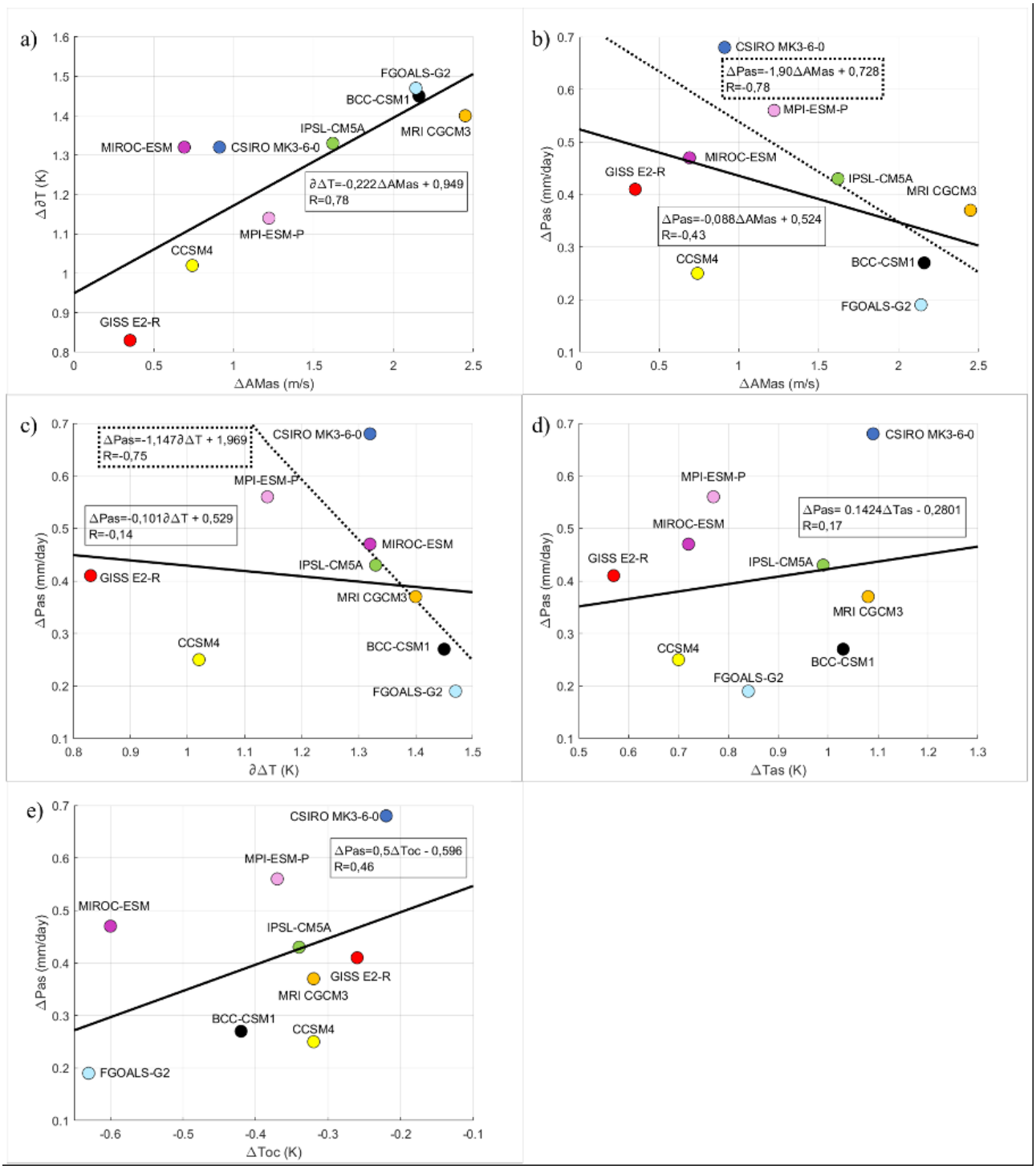

Figure 2 Link between seasonal mean of (a) ASM wind (ΔAMas) with continent-ocean thermal gradient (∂ΔT), Asian summer rainfall (ΔPas) with (b) ASM wind (ΔAMas), (c) continent-ocean thermal gradient (∂ΔT), (d) Asian surface temperature (ΔTas), and (e) Indian Ocean SST (ΔToc) for the mid-Holocene minus pre-Industrial as simulated by the nine GCMs from PMIP3. Solid lines are based on the linear regression of all GCMs, while dashed lines are regressed without CCSM4 and GISS E2-R (b,c). Text boxes contain correlation scores and linear equations of the nearest regression line.

NASA GISS-E2-R reveal noticeable distances compared to the other models. Thus, two regressions were conducted, solid line is the regression line based on all models (R=~-0.14), while the dashed line is the regression devoid CCSM4 and NASA GISS-E2-R (R=~-0.75). Negative correlation scores demonstrate that Asian rainfall variability are inversely proportional to the variability of the continent-ocean thermal gradient. It suggests that a model with small changes of the thermal gradient will have much enhanced rainfall over Asia. From a group model without CSSM4 and NASA GISS-E2-R, the smallest change of the thermal gradient (1.14K) was

simulated by MPI-ESM-P, resulting maximum rainfall of 0.56 mm/day. While the largest variability of thermal gradient (1.47K) was simulated by FGOALS-G2, resulting minimum rainfall of 0.19 mm/day.

Anti-correlation between thermal gradient and Asian monsoon wind with rainfall derived from the result in Figure 2(b) and 2(c) might be related to the variability of surface temperature either in Asia or Indian Ocean. Thus, multi-model variations between each surface temperature with Asian rainfall were also investigated. Figure 2(d) displays multi-model variation of the Asian surface temperature and Asian rainfall. The two quantities have a weak relationship since their correlation score is ~0.17. From the plot, NASA GISS-E2-R reveals the minimum Asian surface temperature up to 0.57 K, however NASA GISS-E2-R does not exhibit minimum rainfall values. Meanwhile CSIRO MK-3-6-0 shows a maximum change in both surface temperature (1.09 K) and rainfall (0.68 mm/day). Figure 2(e) represents multi-model variation of the Indian Ocean SST and Asian rainfall. Multi-model variation in Figure 2(e) demonstrates positive correlation score of ~0.45 which are higher than the one shown in Fig 2(d). FGOALS-G2 is a model that simulates the largest change in Indian Ocean SST at -0.63K, in contrast CSIRO MK-3-6-0 simulates the least change of SST at -0.22K.

DISCUSSION

All models showed significant changes in all of their involved physical quantities between the mid-Holocene and pre-Industrial simulations (Table 2). Those changes are the increase in continent-ocean thermal gradient, Asian rainfall intensity, ASM wind and Asian surface temperature; and a decrease in the Indian Ocean SST. Warmer (colder) than pre-Industrial surface temperature (SST) in Asia (Indian Ocean) during the mid-Holocene is considered as the implication of the stronger insulation during mid-Holocene compared to that during pre-Industrial on the northern Hemisphere during boreal summer (Polanski et al., 2012). Thus, changes in surface temperature in Asian continent and Indian Ocean are expected to change the thermal gradient between the two locations. These results are consistent with previous studies, which exhibit a larger-than-today inter-hemispheric thermal gradient under a stronger-than-today insolation during the mid-Holocene (Wohlfahrt et al., 2004; Zheng et al., 2013). Stronger ASM wind during the mid-Holocene is also consistent with proxy study about the strengthening of ASM during the mid-Holocene based on lake sediment records from Central Himalaya (Rawat et al., 2021).

During mid-Holocene, each model reveals stronger ASM wind and ocean-continent thermal gradient compared to these during the pre-Industrial (Table 2). Furthermore, variation of GCMs demonstrate a strengthening of the ASM wind in association with the increase of continent-ocean thermal gradient. Thus, the correlation score of the multi-model variation suggests that models with the largest increase in temperature gradient resulting the largest increase in their ASM wind. This result is consistent with the monsoon theory, which noted that the higher temperature gradient leads to the higher wind speed (Desai et al., 2009).

Multi-model variation between changes in ASM wind and continent-ocean thermal gradient with the changes in Asian rainfall indicate an inverse correlation, particularly when GISS E2-R and CCSM4 are excluded (Figure 2b and 2c). This result implies that models with the smallest increase in ASM wind and temperature gradient lead to greater rainfall over Asia. This inverse correlation is inconsistent with the general understanding of the ASM variability (Cheng et al., 2016b; Ren et al., 2021; Schneider et al., 2014). ASM wind and rainfall are known to vary in-coherent with continent-ocean thermal gradient as their main driver. Thus, the discrepancy between multi-model variation with the general understanding of ASM indicates serious issues may actually be occurred by the multi-model. Previous research has also found a misdistribution of the GCMs in comparison with proxies for the relationship between El Nino Southern Oscillation (ENSO) with seasonal cycle (Emile-Geay et al., 2015). In conclusion, multi-model variation actually encounters various issues, and one of them is observed by our study.

The inverse correlation may actually be caused by the changes of the Indian Ocean SST (which indicates cooling trend) since it is a negative factor in Equation 3. This is confirmed by the multi-model analyses which demonstrated that a stronger-than-today Asian rainfall during the mid-Holocene is more correlated with less cold than-today Indian Ocean SST rather than with much warmer-than-today Asian surface temperature. Such relationship is further confirmed by the scores of their partial correlations, which emphasized the independent effect of each surface temperatures to the Asian rainfall by eliminating the other influences. Changes of the Indian Ocean SST has a partial correlation up to ~0.43 with the changes of the rainfall in Asian continent. While the partial correlation between changes of surface temperature in the Asian continent with the changes in Asian rainfall is only ~0.1. Thus, a model that simulates a less cold-than-today Indian Ocean SST produces a much wetter-than-today Asian climate during the mid-Holocene.

Multi-model analyses revealed the significant role of Indian Ocean SST in changing rainfall over Asian continent in orbital time scale (Figure 2e). Correlation of the multi-model variation between the two parameters shows that a less cold SST in the Indian Ocean produces a much higher rainfall over Asia. In order to speculate on the underline mechanism, we may assume that model with less cold SST on the Indian Ocean might also have more areas of unchanged or even warmer SST. The unchanged and/or warmer SST might be related to the moisture supply of the ASM which is associated with the evaporation in the Indian Ocean. In boreal summer, evaporation in Indian Ocean is the source of horizontal

moisture flux and ASM eventually. Thus, a less cold Indian Ocean SST will have a less suppressed evaporation on the ocean surface. Surface evaporation in Indian Ocean gives a contribution to the supply of the atmospheric water vapor, which is the source of rainfall in Asia.

Positive correlation between Indian Ocean SST and rainfall over Indian sub-continent are already known to occur within biennial (2-3 years) time-scales (Li et al., 2001). Long-term positive anomaly of the SST in some part of the Indian Ocean increases surface moisture due to the increase in evaporation. As a consequence, a heavy monsoon rainfall over Indian sub-continent occurred resulted from stronger moisture fluxes into the ASM region. Similar mechanism, but in an orbital time-scale, could be suggested to explain the role of Indian Ocean SST in increasing Asian rainfall, simulated in our multi-model analyses. Model with a less cold Indian Ocean SST suppresses much less evaporation compared to the other models do. This perhaps due to more pockets of unchanged/warmer SST. Along these lines, our speculated mechanisms are in accordance to the results of the multi-model. CESS FGOAL-S2 is a model that apply the coldest Indian Ocean SST to simulate a smallest increase of Asian rainfall. While CSIRO MK-3-6-0 is a model that shows the least cold SST simulates a much higher Asian rainfall. Thus, moisture content dynamic over the Indian Ocean is important for the increase of ASM during the mid-Holocene climate change relative to the pre-Industrial.

Correlation score of the multi-model variation between higher-than-today Asian rainfall to the colder-than-today Indian Ocean SST (~-0.45) is higher than the one with the warmer-than-today Asian continent (~0,17) (Fig. 2c & 2d). However, warmer-than-today Asian continent remains arguably important since the correlation between the higher-than-today Asian rainfall to the changes of continent-ocean thermal gradient (~-0.75) is much higher than the one with the Indian Ocean SST (Fig. 2b & 2c). Such a high correlation score emphasizes on the important role of a warmer-than-today Asian continent in the multi-model variation, based on the calculation of the continent-ocean thermal gradient (Equation 3). Further investigation of multi-model variation of the ever-changing ASM throughout various climate scenarios remains crucial to get a better understand multi-model behavior, which is needed to evaluate the precision of the future climate projection (Chhin & Yoden, 2018).

CONCLUSIONS

This research can be concluded that the changes in continent-ocean thermal gradient has a positive correlation with ASM wind. However, a negative correlation occurs between changes in continent-ocean thermal gradient with Asian rainfall. Models that simulate large changes in the continent-ocean thermal gradient produce the smallest increase in the Asian rainfall and vice versa. Such inverse relation is likely due to the cooling of Indian Ocean SST since its correlation scores with Asian rainfall is much higher than the one with the warming of the Asian continent. Thus, multi-model variation of the increased rainfall over the Asian continent between mid-Holocene and today is mainly related to the multi-model variation of the cooling in the Indian Ocean SST.

ACKNOWLEDGEMENTS

This research is part of projects titled “Marine Science & Technology Cooperation between Korea and Indonesia (20180319)” and “Ocean and Coastal Basic Survey and Capacity Enhancement in Cirebon, Indonesia (G52440)” which are funded by the Ministry of Oceans and Fisheries, Korea.

AUTHOR CONTRIBUTION

Adinda Maharani acquired and analyzed all GCMs simulations output from the PMIP3 online database, and also wrote the manuscript. Yudha Setiawan Djamil proposed the main idea, designed the analytical approach, and actively involved in the discussion, also correction and comments on the manuscript. Thus, Adinda Maharani and Yudha Setiawan Djamil are considered as the main contributors of this manuscript. Author member: Rima Rachmayani contributes to the discussion of the main idea, gave permission to use computer equipment for data processing, also correction and comments on the manuscript.

REFERENCES

Bartlein, P. J., Harrison, S. P., Brewer, S., Connor, S., Davis, B. A. S., Gajewski, K., Guiot, J., Harrison-Prentice, T. I., Henderson, A., Peyron, O., Prentice, I. C., Scholze, M., Seppa, H., Shuman, B., Sugita, S., Thompson, R. S., Viau, A. E., Williams, J., & Wu, H. 2011. Pollenbased continental climate reconstructions at 6 and 21 ka a global synthesis. *Climate Dynamics*, 37(3–4): 775–802. https://doi.org/10.1007/s00382-010-0904-1.

Berger, A. 1978. Long-term variations of daily insolation and Quaternary climatic changes. *Journal of the Atmospheric Sciences*, 35(12): 2362–2367.

Braconnot, P., Denvil, S., Foujols, M. A., Caubel, A., Marti, O., Dufresne, J.-L., Bopp, L., Cadule, P., Ethé, C., Idelkadi, A., Mancip, M., Masson, S., Mignot, J., Ionela, M., Balkanski, Y., Bekki, S., Bony, S., Brockman, P., Codron, F.,Vuichard, N. 2016. *IPSL-CM5A-LR model output prepared for CMIP5 midHolocene experiment, served by ESGF*. World Data Center for Climate (WDCC) at DKRZ. https://doi.org/https://doi.org/10.1594/WDCC/CMIP5.IPILmh. https://www.wdc-climate.de/ui/ accessed at 2021-08-20.

Braconnot, P., Marti, O., Joussaume, S., & Leclaineche, Y. 2000. Ocean Feedback in Response to 6 kyr BP Insolation. *Journal of Climate*, 13: 1537–1553.

Chen, F., Yu, Z., Yang, M., Ito, E., Wang, S., Madsen, D. B., Huang, X., Zhao, Y., Sato, T., Birks, H. J. B., Boomer, I., Chen, J., An, C., & Wunnemann, B. 2008. Holocene moisture evolution in arid central Asia and its out-of-phase relationship with Asian monsoon history. *Quaternary Science Reviews*, 27: 351–364. https://doi.org/10.1016/j.quascirev.2007.10.017.

Cheng, H, Edwards, R., Sinha, A., Spötl, C., Yi, L., Chen, S., Kelly, M., Kathayat, G., Wang, X., Li, X., & Kong, X. 2016a. The Asian monsoon over the past 640,000 years and ice age terminations. *Nature*, 534(7): 609–640.

Cheng, H., Spötl, C., Breitenbach, S. F. M., Sinha, A., Wassenburg, J. A., Jochum, K.P., Scholz, D., Li, X., Yi, L., Peng, Y., Lv, Y., Zhang, P., Votintseva, A., & Loginov, V., 2016b. Climate variations of Central Asia on orbital to millennial timescales. *Scientific Reports,* 5: 36975. DOI: 10.1038/srep36975. PMID: 27833133; PMCID: PMC5105073.

Cheng, J., Wu, H., Chen, H., Lu, H., Liu, Z., Gu, P., Wang, J., Zhao, C., & Li, Q. 2021. Vegetation feedback causes delayed ecosystem response to East Asian Summer Monsoon Rainfall during the Holocene. *Nature Communications*. https://doi.org/10.1038/s41467-021-22087-2.

Chhin, R., & Yoden, S. 2018. Ranking CMIP5 GCMs for model ensemble selection on regional scale: case study of the Indochina Region. *Journal of Geophysical Research: Atmospheres*, 123(17): 8949–8974.

Dallmeyer, A. and Claussen, M., 2011. The influence of land cover change in the Asian monsoon region on present-day and mid-Holocene climate. *Biogeosciences,* 8: 1499-1519. 10.5194/bg-8-1499-2011.

Desai, A. R., Austin, J. A., Bennington, V., & Mckinley, G. A. 2009. Stronger winds over a large lake in response to weakening air-to-lake temperature gradient. *Nature Geoscience*, 2(12): 855–858.

Ding, Y., & Chan, J. C. L. 2005. The East Asian summer monsoon : an overview. *Meteorog. Atmos. Phys*, 142: 117–142. https://doi.org/doi.org/10.1007/s00703-005-0125-z.

Emile-Geay, J., Cobb, K. M., Carré, M., Braconnot, P., Leloup, J., Zhou, Y., Harrison, S. P., Corrège, T., Mcgregor, H. V, Collins, M., Driscoll, R., Elliot, M., Schneider, B., & Tudhope, A. 2015. Links between tropical Pacific seasonal, interannual and orbital variability during the Holocene. *Nature Geoscience*, 1–7. https://doi.org/10.1038/ngeo2608.

Hewitt, C. D., & Mitchell, J. F. B. 1996. GCM Simulations of Climate of 6 kyr BP: Mean Changes and Interdecadal Variability. *Journal of Climate*, 9: 3505–3529.

<https://www.wdc-climate.de/ui/> [Accessed at 20 August 2021].

<https://wiki.lsce.ipsl.fr/pmip3/doku.php/310822 - BoMG_Vol37_No1_Jatiningrum_etalpmip3:database:status> [Accessed at 4 May 2022].

JAMSTEC, AORI, & NIES. 2015. *MIROC-ESM model output prepared for CMIP5 midHolocene, served by ESGF*. World Data Center for Climate (WDCC) at DKRZ. https://doi.org/https://doi.org/10.1594/WDCC/CMIP5.MIMEmh. https://www.wdc-climate.de/ui/ accessed at 2021-08-20.

Jeffrey, S., Rotstayn, L., Collier, M., Dravitzki, S., Hamalainen, C., Moeseneder, C., Wong, K., & Syktus, J. 2016. *CSIRO-Mk3-6-0 model output prepared for CMIP5 midHolocene (Version 2015), served by ESGF*. World Data Center for Climate (WDCC) at DKRZ. https://doi.org/https://doi.org/10.1594/WDCC/CMIP5.CQMKmhv2015. https://www.wdc-climate.de/ui/ accessed at 2021-08-20.

Jiang, D., Tian, Z., & Lang, X. 2013. Mid-Holocene net precipitation changes over China : model e data comparison. *Quaternary Science Reviews*, 82: 104–120. https://doi.org/10.1016/j.quascirev.2013.10.017.

Joussaume, S., Taylor, K. E., Braconnot, P., Mitchell, J. F. B., Kutzbach, J. E., Harrison, S. P., Prentice, I. C., Broccoli, A. J., Abe-Ouchi, A., Bartlein, P. J., Bonfils, C., Dong, B., Guiot, J., Henerich, K., Hewitt, C. D., Jolly, D., Kim, J. W., Kislov, A., Kitoh, A., Wyputt, U. 1999. Monsoon changes for 6000 years ago: Results of 18 simulations from the Paleoclimate Modeling Intercomparison Project (PMIP). *Geophysical Research Letters*, 26(7): 859–862.

Jungclaus, J., Giorgetta, M., Reick, C., Legutke, S., Brovkin, V., Crueger, T., Esch, M., Fieg, K., Fischer, N., Glushak, K., Gayler, V., Haak, H., Hollweg, H.-D., Kinne, S., Kornblueh, L., Matei, D., Mauritsen, T., Mikolajewicz, U., Müller, W., Stevens, B. 2012. *CMIP5 simulations of the Max Planck Institute for Meteorology (MPI-M) based on the MPI-ESM-P model: The midHolocene experiment, served by ESGF*. World Data Center for Climate (WDCC) at DKRZ. https://www.wdc-climate.de/ui/ accessed at 2021-08-20.

LASG, Institute of Atmospheric Physics, C. A. of S. (IAP-L. 2015. *FGOALS-g2 model output prepared for CMIP5 midHolocene, served by ESGF*. World Data Center for Climate (WDCC) at DKRZ. https://doi.org/https://doi.org/10.1594/WDCC/CMIP5.LSF2mh. https://www.wdc-climate.de/ui/ accessed at 2021-08-20.

Li, T., Chang, C., & Wang, B. 2001. On the relationship between Indian Ocean sea surface temperature and Asian Summer Monsoon. *Geophysical Research Letters*, 28(14): 2843–2846.

Mahowald, N. M., Yoshioka, M., Collins, W. D., Conley, A. J., Illmore, D. W., & Coleman, D. B. 2006. Climate response and radiative forcing from mineral aerosols during the last glacial maximum, pre-industrial, current and doubled-carbon dioxide climates. *Geophysical Research Letters*, 33(20): 1-4.

NASA Goddard Institute for Space Studies (NASA/GISS). 2014. *NASA-GISS: GISS-E2-R model output prepared for CMIP5 mid-Holocene, served by ESGF.* World Data Center for Climate (WDCC) at DKRZ. https://doi.org/https://doi.org/10.1594/WDCC/CMIP5.GIGRmh. https://www.wdc-climate.de/ui/ accessed at 2021-08-20.

Ohgaito, R. & Abe-Ouchi, A., 2007. The role of ocean thermodynamics and dynamics in Asian summer monsoon changes during the mid-Holocene. *Climate Dynamic,* 29: 39-50. 10.1007/s00382-006-0217-6.

Otto-Bliesner, B. 2014. *CCSM4 coupled simulation for CMIP5 with mid-Holocene conditions, served by ESGF*. World Data Center for Climate (WDCC) at DKRZ. https://doi.org/https://doi.org/10.1594/WDCC/CMIP5.NRS4mh. https://www.wdc-climate.de/ui/ accessed at 2021-08-20.

Polanski, S., Rinke, A., Dethloff, K., Lorenz, S. J., Wang, Y., & Herzschuh, U. 2012. Simulation and comparison between mid-Holocene and Pre-Industrial Indian summer monsoon circulation using a regional climate model. *The Open Atmospheric Science Journal*, 6: 42–48.

Rao, Z., Jia, G., Li, Y., Chen, J., Xu, Q., & F., C. 2016. Asynchronous evolution of the isotopic composition and amount of precipitation in north China during the Holocene revealed by a record of compound-specific carbon and hydrogen isotopes of long-chain n-alkanes from an alpine lake. *Earth and Planetary Science Letters*, 466: 68–76. https://doi.org/10.1016/j.epsl.2016.04.027.

Rawat, V., Rawat, S., Srivastava, P., Negi, P. S., Prakasam, M., & Kotlia, B.S. 2021. *Middle Holocene Indian summer monsoon variability and its impact on cultural changes in the Indian subcontinent*. *Quaternary Science Reviews, 255(2021)*.https://doi.org/10.1016/j.quascirev.2021.106825.

Ren, X., Sha, Y., Shi, Z., & Liu, X. 2021. Response of summer extreme precipitation over East Asia during the mid-Holocene versus future global warming. *Global and Planetary Change*, 197: 103–398.

Schneider, T, Bischoff, T., & Haug, G. H. 2014. Migrations and dynamics of the intertropical convergence zone. *Nature*, 513(7516): 45–53.

Tao, W., Huijun, W., & Dabang, J. 2010. Mid-Holocene East Asian summer climate as simulated by the PMIP2 models. *Palaeogeography, Palaeoclimatology, Palaeoecology*, 288(1–4): 93–102. https://doi.org/10.1016/j.palaeo.2010.01.034.

Wang, B., & Fan, Z. 1999. Choice of South Asian Summer Monsoon Indices. *Bulletin of the American Meteorological Society,* 80(4): 629–638.

Wang, B., R, Wu., K-M, Lau. 2001. Inter Annual variability of Asian summer monsoon: contrast between the Indian and western North Pacific-East Asian monsoon. *Journal of Climate,*14: 4073-4090.

Wen, R., Xiao, J., Chang, Z., Zhai, D., Xu, Q., Li, Y., Itoh, S., & Lomtatidze, Z. 2010. Holocene climate changes in the mid-high-latitude-monsoon margin re fl ected by the pollen record from Hulun Lake , northeastern Inner Mongolia. *Quaternary Research*, 73(2): 293–303. https://doi.org/10.1016/j.yqres.2009.10.006.

Wohlfahrt, J., Harrison, S. P., & Braconnot, P. 2004. Synergistic feedbacks between ocean and vegetation on mid- and high-latitude climates during the mid-Holocene. *Climate Dynamics*, 22: 223–238.

Wu, T., & Xin, X. 2015. *bcc-csm1-1 model output prepared for CMIP5 midHolocene experiment, served by ESGF*. World Data Center for Climate (WDCC) at DKRZ. https://doi.org/https://doi.org/10.1594/WDCC/CMIP5.BCB1mh. https://www.wdc-climate.de/ui/ accessed at 2021-08-20.

Xiao, J., Chang, Z., Wen, R., Zhai, D., Itoh, S., & Lomtatidze, Z. 2009. Holocene weak monsoon intervals indicated by low lake levels at Hulun Lake in the monsoonal margin region of northeastern Inner Mongolia , China. *Holocene*, 19: 899–908.

Yafeng, S., Zhaozheng, K., Sumin, W., Lingyu, T., Fubao, W., Tandong, Y., Xitao, Z., Peiyuan, Z., & Shaohua, S. 1993. Mid-Holocene climates and environments in China. *Global and Planetary Change*, 7(1–3): 219–233.

Yukimoto, S., Adachi, Y., Hosaka, M., Sakami, T., Yoshimura, H., Hirabara, M., Tanaka, T., Shindo, E., Tsujino, H., Deushi, M., Mizuta, R., Yabu, S., Obata, A., Nakano, H., Koshiro, T., Ose, T., & Kitoh, A. 2015. *MRI-CGCM3 model output prepared for CMIP5 midHolocene, served by ESGF.* World Data Center for Climate (WDCC) at DKRZ. https://doi.org/https://doi.org/10.1594/WDCC/CMIP5.MRMCmh. https://www.wdc-climate.de/ui/ accessed at 2021-08-20.

Zhao, Y., Braconnot, P., Marti, O., Harrison, S. P., Hewitt, C., Kitoh, A., & Weber, S. L. 2005. A multi-model analysis of the role of the ocean on the African and Indian monsoon during the mid-Holocene. *Climate Dynamics*, 25(7–8): 777–800. https://doi.org/10.1007/s00382-005-0075-7.

Zheng, B., Wu, J., He, Y., & Yu. 2013. The East Asian Summer Monsoon at mid-Holocene: results from PMIP3 simulations. *Climate Past*, 9: 453–466. https://doi.org/10.5194/cp-9-453-2013.